A Simple and Effective Approach to Real-Time Ionospheric Monitoring for GBAS in Low Latitudes

Leonardo Marini-Pereira, *Institute of Airspace Control*
Alison de Oliveira Moraes, *Institute of Aeronautics and Space*
Sam Pullen, *Stanford University*

BIOGRAPHIES

Dr. Leonardo Marini-Pereira is a Research Engineer at the Institute of Airspace Control (ICEA) in Brazil managing scientific research related to technologies of the Brazilian Airspace Control System. His research interests include GNSS-based technologies for air navigation and analysis of ionospheric effects on GNSS in low latitudes.

Dr. Alison de Oliveira Moraes is a Senior Technologist with the Institute of Aeronautics and Space (IAE) in Brazil. His research interest includes statistical models for ionospheric radio signals, low-cost platforms for science dissemination, avionics, and space systems engineering.

Dr. Sam Pullen is a Senior Research Engineer with the GPS/GNSS Laboratory in the Aeronautics and Astronautics Department at Stanford University. His research focuses on system integrity assurance and design optimization under uncertainty, especially for users of Global Satellite Navigation Systems (GNSS) and augmentations such as Ground and Satellite-based Augmentation Systems (GBAS and SBAS).

ABSTRACT

This paper proposes a strategy to improve the performance of Ground-Based Augmentation Systems (GBAS) in low latitudes. A methodology was developed for an alerting system that uses surrounding ground stations to monitor the ionosphere state in real time and send alerts to a GBAS facility when threatening conditions are detected. The method is based on time-step gradients used as a test statistic along with data gap analysis to detect ionospheric disturbances and declare periods for affected satellite signals to be declared unavailable. The method for translating detections of threatening conditions into alerts to not use specific satellites depends on three different parameters, and 30 different combinations of these were tested. Validation was performed with real data using the largest observed gradients that form the Brazilian ionospheric threat model. The results demonstrated that the method is highly effective, detecting the vast majority of previously known threatening gradients within a maximum temporal tolerance of 5 minutes. An availability assessment was also performed to check for availability outages resulting from the application of the technique. These outage periods varied significantly with day of year and location. Cases were found in which all threatening gradients were detected without loss of availability. However, in the worst case, the application of the alerting method with the most sensitive set of parameters resulted in an outage period of approximately 5 hours using monitoring stations in the region of the city of Salvador, Brazil. Despite such loss of availability in the worst-case outage, this result is far better than declaring the system totally unavailable every night (when equatorial plasma bubbles typically occur). The application of the developed technique has the potential to improve low-latitude nighttime GBAS availability.

1   INTRODUCTION

The Ground-Based Augmentation System (GBAS) is a safety-critical navigation aid designed to provide precision approach service in low-visibility conditions. One of the key unresolved issues for low-latitude GBAS implementation is potential loss of integrity

due to spatial decorrelation between the corrections provided by a GBAS ground station and airborne receivers. This phenomenon is caused by the ionospheric layer's influence on Global Navigation Satellite System (GNSS) signals.

Threatening ionospheric gradients that create integrity risk for GBAS cannot be detected by the ground station alone in real time. Given this limitation, the most common mitigation procedure for existing GAST C GBAS installations supporting Category I (CAT I) precision approaches is position-domain geometry screening, or PDGS (Lee et al., 2011), which assumes that the worst ionospheric condition (from the point of view of integrity risk) defined by a regional ionospheric threat model is always present. While this technique reduces availability due to this conservative assumption, the resulting CAT I GBAS availability is acceptable in mid-latitude regions.

However, the ionosphere in low-latitude regions, which includes Brazil, has intense dynamics with considerable variability (Sousasantos et al., 2021). The most critical effect found in those regions is signal scintillation due to plasma bubbles in the ionosphere. For an augmentation system like GBAS, plasma bubbles can generate gradients in ionospheric delay large enough to compromise the system's integrity, resulting in unsafe operation.

In order to use PDGS at a GBAS facility in Brazil, the Brazilian Department of Airspace Control (DECEA) supported the development of a GBAS ionospheric threat model for Brazil (Lee et al., 2015; Yoon et al., 2017a). The effort relied on a multidisciplinary group of researchers that evaluated and validated the occurrence of gradients in Brazil from multiple GNSS networks. The results showed that threatening gradients are a recurrent scenario in Brazil, as reported, for example, in Affonso et al. (2022) and Yoon et al. (2020). The most threatening gradients were found to be more than twice the ones from the Conterminous United States (CONUS) ionospheric threat model (Datta-Barua et al., 2010). Considering such high gradients in the position-domain geometry screening can significantly degrade GBAS availability in low latitudes, as assessed by Yoon et al. (2016, 2019).

A means for detecting and alerting GBAS ground facilities about the presence of threatening ionospheric events, including plasma bubbles, would be of great value to guarantee integrity with minimum loss of availability. Hence, this paper proposes a methodology capable of monitoring the ionosphere state in real time by using ground monitor stations external to GBAS but near GBAS facilities. The technique is based on time-step gradients used as a test statistic along with data gap analysis to detect threatening conditions and declare periods for affected satellite signals to be unavailable. The method for translating detection of threatening conditions into alerts to not use specific satellites depends on three different parameters, and 30 different combinations of them were tested. Validation was performed with real data using known ionospheric gradients from the Brazilian ionospheric threat model.

2   REAL-TIME IONOSPHERIC MONITORING CONCEPT

Augmentation systems for precision air navigation procedures are challenging to implement in low latitudes due to the impact of ionospheric variability (Marini-Pereira et al., 2021). For GBAS, the current architecture for GAST C is not ideally suited to the low-latitude environment and suffers a significant loss of availability (compared to mid latitudes) due to the likelihood of threatening ionospheric conditions. While the use of two signal frequencies and multiple GNSS constellation seems to be the most viable solution, it presents other issues, such as more susceptibility to scintillation and increased noise levels (Felux et al., 2017; Gerbeth et al., 2016; Salles et al., 2021). Also, the standards for using dual-frequency augmentation systems are likely to remain unfinished for the next few years, at least for GBAS.

The new methodology for detecting threatening ionospheric events for GBAS in real-time proposed in this paper is based on use of existing GNSS monitoring networks. Applying a method that can work in real-time with networks of lower-cost receivers faces considerable challenges, including additional complexity. Hence, proving the concept of a methodology applicable in real time and able to mitigate GBAS availability in low latitudes is one of the core contributions of this paper.

2.1   System definition

The proposed concept for an eventual alerting system requires a network of monitoring reference stations around a GBAS facility within a certain radius, as illustrated in Figure 1. The reference stations' role is to monitor the ionosphere based on specific parameters and thresholds and send alerts to the supported GBAS facility when GBAS should make specific satellites unavailable (i.e., stop broadcasting corrections for them) due to threatening ionospheric conditions. The proposed methodology is similar to the idea presented by Caamano et al. (2019, 2021) regarding the test statistic and the disposition of monitoring stations around a GBAS facility to issue alerts during threatening conditions. However, the method proposed herein is much less complex than the one proposed by Caamano et al. (2019, 2021) that used simulated and empirical high-latitude data. Also, the method presented in this paper has its performance assessed using actual low-latitude data.
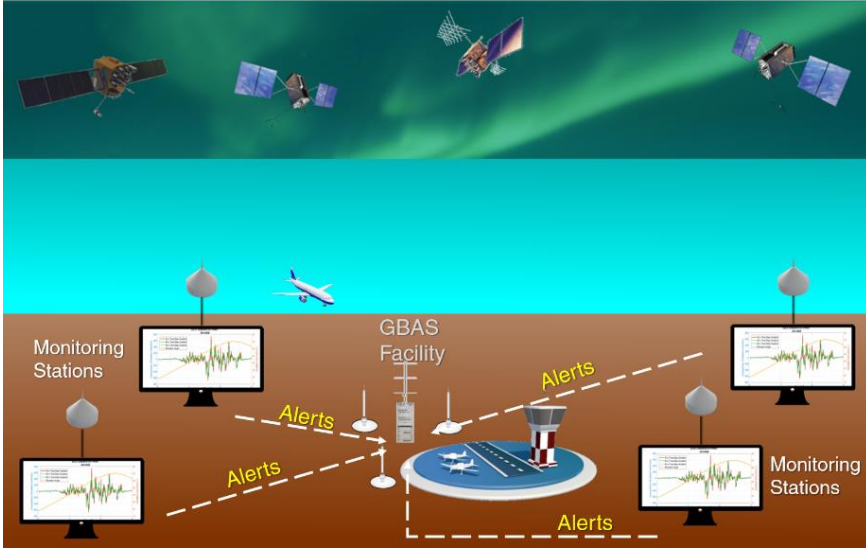
Figure 1
General concept of the GBAS alerting system

The experiments presented in this work are performed by means of data from existing monitoring networks, which was suggested by Pullen et al. (2010) when proposing the use of ionospheric error bounds provided by an SBAS covering the region of interest of a GBAS station. In addition, the cited authors suggest that their proposed strategy can be applied in regions outside of good SBAS coverage using available uncertified monitoring networks. Issues and concerns of using uncertified networks for an aviation system are discussed by Pullen et al. (2010), but they are out of the scope of this work, which aims to demonstrate a methodology concept instead of developing a certifiable system.

2.2 Computation of the test statistic

The test statistic chosen for the proposed alerting methodology is based on time-step estimates of ionospheric gradients. In low latitude regions, such as Brazil, the ionosphere has enormous variability, and baselines (receiver antenna separations) longer than 50 km may not properly capture spatial-gradient behavior. Since the available reference stations in Brazil are widely separated, the time-step method is an attractive alternative.

The time-step method was introduced by Datta-Barua et al. (2002) using WAAS reference stations, which are hundreds of kilometers apart. It was also applied by Yoon et al. (2015, 2017b, 2020) as a means to validate gradients estimated by the station-pair method to develop the Brazilian ionospheric threat model for GBAS. It is computed by a single station m and a single satellite n with measurements of slant ionospheric delay I_m^n separated by a time step Δ_t and divided by the distance D_{ipp} between the Ionospheric Pierce Points (IPP) at the epochs considered (t and $t - \Delta_t$) as follows:

$$\nabla I_{ts}(t) = \frac{I_m^n(t) - I_m^n(t - \Delta_t)}{D_{ipp}} \tag{1}$$

Equation (1) has the advantage of eliminating both receiver and satellite hardware bias, so neither bias is required to be estimated. However, the time-step method includes the temporal gradient between the two different epochs in addition to the spatial gradient. The Δ_t parameter plays a key role when determining these gradients. It directly affects the baseline distance between the IPPs, with longer distances for longer time intervals, and longer time intervals give more temporal decorrelation as well. The effect of varying the IPP separation distance for the vertical ionospheric delay calculation is discussed by Chang et al. (2021, 2019) with respect to estimating the nominal σ_{vig} using the time-step method.

One aspect worth mentioning is that the distances will be longer for low satellite elevations and shorter for high elevations. Since the ionospheric delays involved are in the slant domain, the larger values at low elevations are compensated by larger distances. The same happens at high elevations, with shorter distances for shorter time steps, resulting in a "normalization effect" for gradients computed by this method. In summary, the variation in satellite elevation angle is not directly captured by ionospheric gradients computed by the time-step method.
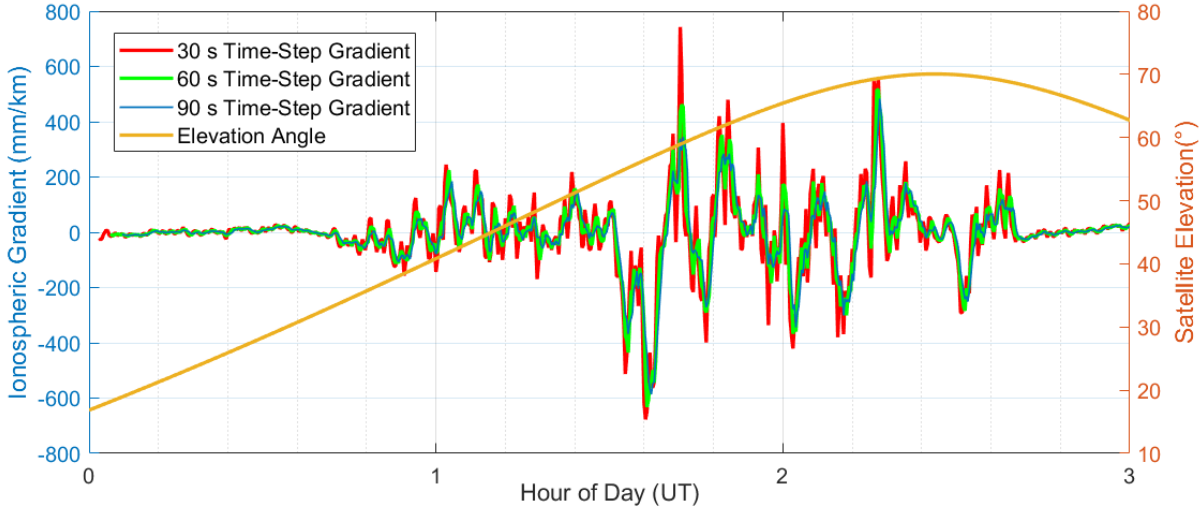
Figure 2
Time-step gradients computed with three different steps. Data from SJCE station on March 1, 2014, for GPS PRN 01.

Also of interest is the fact that longer time steps naturally result in longer IPP separations. For the same ionospheric measurements and conditions, shorter time steps generally yield larger gradients, and longer time steps yield smaller gradients. Figure 2 illustrates an example using a three-hour temporal plot of time-step gradients expressed in mm/km, computed with three different Δ_t for the same satellite (GPS PRN 01), along with the evolution of its elevation angle. The magnitude of the gradients indicates a possible ionospheric irregularity, and the elevation angle shows no direct effect on the gradients. As explained above, when operating on the same ionospheric delay pattern (such as the one shown in Figure 2, shorter time steps result in larger gradients, and longer time steps yield smaller gradients. Gradients computed using longer time steps are naturally delayed with respect to gradients based on shorter Δ_t, and a "smoothing effect" is noted as time increases. This effect is more evident for larger gradients.

The choice of Δ_t depends on the length of the baseline that is intended to be analyzed. Yoon et al. (2015, 2017b, 2020) used a 60-second step for estimating time-step gradients to validate station-pair measurements. The authors argue that the chosen time corresponds to IPP baselines up to a few kilometers, which is useful for investigating ionospheric gradients in the irregular low-latitude ionospheric environment.

From the presented discussion and the example in Figure 2, it is inferred that the Δ_t parameter determines the sensitivity to detecting ionospheric events when using the time-step method to compute gradients. Considering the behavior of the three time-steps, based on several plots generated like Figure 2, gradients computed with Δ_t of 30 seconds seem to be more suitable to detect ionospheric irregularities, and for this reason, it was the time interval empirically chosen to compute the test statistic as presented.

2.3 Ionospheric delay smoothing

The use of code-derived ionospheric delays is more suitable for real-time applications since they are not ambiguous, as are carrier-derived delays. However, the main disadvantage of code-derived measurements is the higher noise level. For this reason, a smoothing filter, widely used in GNSS receivers and applications was implemented to smooth the code-derived measurements using carrier-derived measurements. A Hatch smoothing filter was applied directly on raw ionospheric estimates I_ρ. The filtered code-derived ionospheric delay $I_{\rho s}$ smoothed by the carrier-derived ionospheric delays I_φ is implemented as:

$$I_{\rho s}(k) = \frac{1}{\nu} I_\rho(k) + \frac{\nu - 1}{\nu} \left[I_{\rho s}(k-1) + I_\varphi(k) - I_\varphi(k-1) \right] \qquad (2)$$

where k is the epoch index, $\nu = k$ when $k < N_s$, and $\nu = N_s$ when $k \geq N_s$. N_s is the maximum number of samples allowed by the filter within the time at which the filter reaches steady state and thus has constant multipliers for both the code and carrier-derived terms, which can also be expressed as a function of a given time constant τ and the receiver sample rate Ts:

$$N_s = \frac{\tau}{Ts} \qquad (3)$$

The time window of the filter, also called the filter time constant, defines the level of smoothing of the measurements since it directly affects the maximum number of samples that influence the filtered result. Longer time constants result in more smoothing of code measurements and thus more noise reduction. However, a high degree of smoothing is less sensitive to rapid variations in the measurements. Such undetected fast changes may represent features of interest to be studied or identified. For this reason, the choice of τ is a trade-off between noise reduction and the ability to capture sudden significant variations.

By analyzing Equation (2), it is clear that the smoothing filter relies on the difference of carrier-derived measurements between two consecutive epochs. If a cycle slip occurs, the filter performance is clearly degraded, contaminating all subsequent measurements. Hence, a cycle slip strategy is required for the application of the filter. The implemented cycle slip detector is applied directly on the carrier-derived ionospheric delays. The algorithm developed for this task is based on Subirana et al. (2013) with additional steps to maximize data availability and prevent erroneous and noisy data due to the filter reset.

Unfortunately, cycle slips are frequent in low latitude ionospheric environments, especially when using weaker signals like semi-codeless GPS L2. Hence, the smoothing of code-derived measurements using carrier-derived measurements becomes more complex and requires frequent resets of the filtering process.

3   DATA PREPARATION

The preparation steps involved in the proposed methodology are depicted in Figure 3, which provides a general view of the processing flow to generate test statistics for each satellite at a single monitoring station in the vicinity of a GBAS facility. From the data collected by the monitoring receivers, code and carrier-derived ionospheric delays are computed. Even though it is not required, all employed measurements are calibrated from the satellites and receivers' estimated hardware biases. Since the method is intended to be applicable in real-time, the bias error estimates for a given day are proposed to be computed with data from the day before.

To achieve trustworthy results and avoid false detections, a screening process is performed on the code-derived ionospheric delays to eliminate clearly erroneous data. Using the "cleaned" output of this procedure, the code delays are smoothed by the carrier delays. Finally, the proposed strategy for the alerting methodology consists of taking advantage of the time-step method outputs as test statistics to detect ionospheric irregularities. The time-step gradients are analyzed against a set of parameters and logical criteria that determine when alerts are issued and how the detected channels (satellites) are handled in GBAS.

At first glance, estimating ionospheric delays, applying the smoothing filter and computing spatial gradients is a straightforward task when using highly stable receivers that generate good-quality measurements. However, using geodetic receivers from uncertified networks not designed for operational monitoring adds extra complexity and require specific issues to be solved. In particular, spurious data and receiver glitches are often found in the data measured by receivers from the networks available for this work. Such issues are mostly concentrated at nighttime during the occurrence of ionospheric irregularities. Data gaps associated with receiver losses of lock, spikes, large jumps, and frequent cycle slips are among the major concerns. When analyzing post-processed data, many of these difficulties can be adequately handled by a variety of techniques. However, dealing with these problems becomes more complex in real-time applications, especially in the low-latitude ionospheric environment.
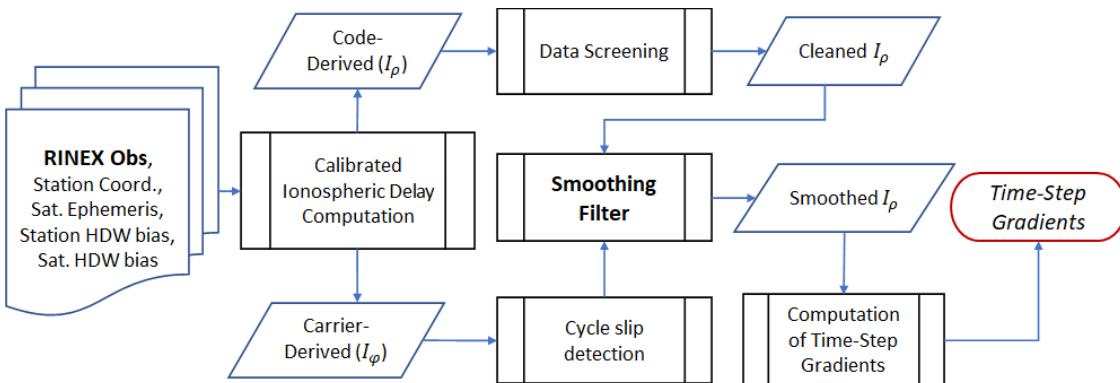

Figure 3
Processing flow of data preparation and generation of the test statistic for each satellite at a single monitoring station

Hence, a strategy was developed to improve the data quality and maximize its availability when spurious measurements or cycle slips are found. These steps are applicable in real-time and were designed to mitigate the impact of erroneous and noisy measurements on the smoothing filter and its subsequent results.

The processing strategy to detect erroneous data is based on defining thresholds to eliminate outliers and data spikes, the latter being defined by two consecutive jumps above a given threshold. In the real-time approach, the spike detection technique delays the detection by twice the data sample rate, since two consecutive epochs are required to analyze consecutive jumps. Thus, considering the 15-second sample rate adopted by the available data, consecutive jump detection reduces the alerting ability to once every 30 seconds. Detected outliers are replaced with the average of measurements from the last 150 seconds, and the detected spikes are replaced with a first-order polynomial fit using measurements from the last 150 seconds. A first-order polynomial fit was chosen to better represent the data trend.

The cleaned code-derived ionospheric delays I_ρ are ready to be used as inputs for the smoothing filter. However, its application requires a cycle slip detection strategy, as the filter depends on carrier-derived measurements. Cycle slip detection is performed on the carrier-derived ionospheric measurements I_φ, combining the implementation used by Jung & Lee (2012) and Subirana et al. (2013). Finally, a strategy to maximize data usage and optimize smoothing was developed to deal with the reset of the smoothing filter when a cycle slip is detected. Instead of using the traditional approach of using the raw code-derived measurement to reset the filter, this method replaces the code-derived measurement of the epoch the cycle slip was found with an interpolated value from raw code measurements over the last 150 seconds. A first-order polynomial fit is used to compute the interpolated value, followed by a residual analysis to detect possible remaining outliers. The output of the data preparation process results in smoothed code-derived ionospheric delays ready to be used as input for the test statistic (time-step gradients).

4   DATASET

The monitoring stations used in this work are from the Continuously Monitoring Brazilian Network (RBMC) – managed by the Brazilian Institute for Geography and Statistics (IBGE) – and the CIGALA network. The latter is the name of the Concept for Ionospheric Scintillation Mitigation for Professional GNSS in Latin America conducted by Unesp University in Presidente Prudente, São Paulo, Brazil devoted to study ionospheric scintillation in Brazil. A few reference stations deployed by ICEA were also used. In all cases, the available data was collected by receivers with 15-second measurement intervals. From these networks, the dataset chosen for this work was based on the observations of very large spatial gradients used to develop the Brazilian GBAS ionospheric threat model. (Lee et al., 2015; Mirus, 2015; Yoon, Lee, et al., 2017a). This dataset encompasses the period between 2011 and 2014 and includes 19 different reference stations. Only gradients in the dataset above 400 mm/km were selected to be processed and used as a validation reference for this work. This lower limit was chosen because it is near the upper limit of the CONUS ionospheric threat model. It is assumed that gradients below this limit can be managed in low latitudes by the CONUS position domain geometry screening technique and the CONUS threat model with a relatively small impact on availability. Thus, the proposed alerting methodology aims to mitigate gradients above this limit.

The most significant gradients used to develop the Brazilian ionospheric threat model were observed by pairs of stations separated by around 10 km and approximately aligned with the geomagnetic equator. Few receivers were available at some locations within a 15 km or 20 km radius. For this reason, the selected dataset forms clusters of stations that will be used in this work as monitoring stations. The map in Figure 4 shows the locations and names (adopted in this work) of the reference stations clusters. Further information about each cluster, such as the number of reference stations and the number of gradients selected from the dataset, is provided in TABLE 1.

The Threat Model dataset is composed of RINEX observation files of the days and stations selected from the Brazilian ionospheric threat model results, which consists of a table with each station-pair gradient magnitude, time of occurrence, pair of station which detected the gradient among other complementary information. Continuous measurements of the station-pair gradients in time are not available for this dataset.
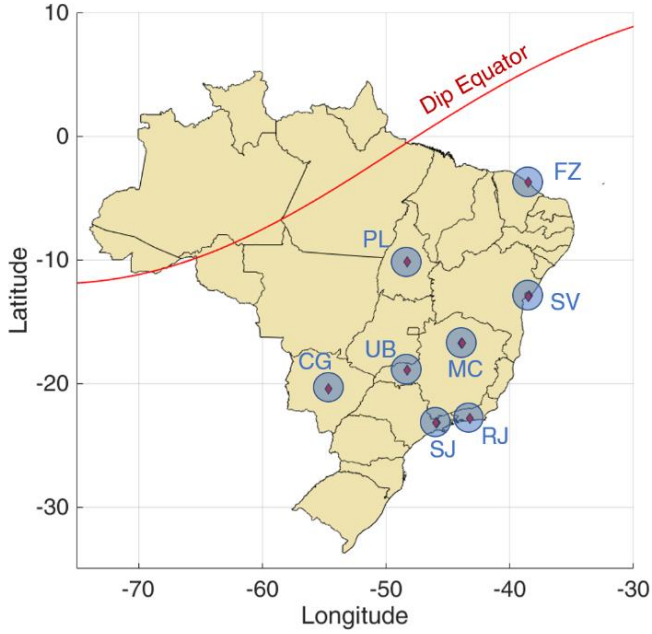
Figure 4
Distribution of the reference stations used in the dataset

TABLE 1
Information for each cluster in the dataset

Cluster Name	Location (City, State)	Number of Stations	Number of Threat. gradients
SV	Salvador, BA	2	31
SJ	São José dos Campos, SP	3	24
FZ	Fortaleza, CE	2	6
MC	Montes Claros, MG	2	5
RJ	Rio de Janeiro, RJ	4	3
CG	Campo Grande, MS	2	1
UB	Uberlândia, MG	2	1
PL	Palmas, TO	2	1

5   ALERTING METHODOLOGY

The key part of the strategy consists of establishing a set of criteria and thresholds for a test statistic to declare alerts based on measured data in real time. First, the test statistic chosen for the alerting algorithm is the 30-second time-step gradient computed in real-time using code-derived ionospheric delays smoothed by carrier-derived ionospheric delays, as described in Figure 3.

With the test statistic, i.e., time-step gradients, computed accordingly, a set of rules must be established to decide when an alert must be issued. Based on the architecture depicted in Figure 1, the proposed methodology will be designed to send alerts to GBAS facilities served by the monitoring stations around it if at least one monitoring station issues an alert. As previously mentioned, the dataset was used to simulate clusters of monitoring stations, as presented in Figure 4.

Using this test statistic, the first parameter of the alerting method is a threshold which will represent the maximum tolerance for the test statistic before an alert is issued. This parameter will be referred to as the Alert Threshold (AT). If the time-step gradient for a given satellite exceeds the pre-defined value for AT, then the GBAS facilities served by the monitoring stations will be under an alert state for that satellite.

Considering the rapid variability of time-step gradients, especially when facing ionospheric irregularities like EPBs, it is undesirable to use a single threshold as the only criterion for declaring or cancelling an alert. Instead, hysteresis is applied using a threshold lower than AT to determine that a particular satellite is no longer under alert. Furthermore, to provide more stability to alerts and avoid frequent changes of status over short time periods, the test statistic must remain under this lower threshold for a given period, beyond which it will be assumed that the threatening condition has passed for the satellite in question. This is when recovery (alert cancellation) actually takes place. The threshold the time-step gradients must be under will be referred to as the Recovery Threshold (RT), and the time the test statistic needs to stay under RT to allow recovery will be referred to as the Time to Recover (TR).

Hence, the steps for declaring an alert using the proposed methodology with the 30-second time-step gradient as test statistic are:

a)   If the test statistic for a satellite exceeds AT, the monitoring station issues an alert for that satellite.

b)   The satellite will remain under alert until its test statistic continuously remains under RT for the period defined by TR.

Additionally, absence of data was also used as an alert criterion since data gaps often occur during disturbed ionospheric periods. Thus, the steps above are performed only when the test statistic is available, i.e., there is no data gap at the current epoch. Hence, data availability is considered a pre-condition to compute the test statistic. In the case of 30-second time-step gradients, three times Δ_t, i.e., 90 seconds of continuous data are required to compute the test statistic. If the absence of data is detected, meaning that there is not at least 90 seconds of continuous measurements of the smoothed code-derived ionospheric delay ($I_{\rho s}$), the satellite is immediately put under alert until the test statistic can be computed again.

The logic of these steps for a single satellite at a single monitoring station is summarized in the flowchart of Figure 5. The green dashed box encompasses the steps performed in normal operation, i.e., the satellite is being used by the GBAS facility if not excluded by the internal GBAS monitors. When the satellite is excluded by this external warning system, i.e., an alert is issued for that satellite, the processing flow occurs within the lower dashed box.

Once the alert threshold is exceeded, the method will monitor the test statistic to check for stability of measurements below the recovery threshold. In other words, the magnitude of the test statistic has no effect on the method once AT is exceeded, unless it is below the recovery threshold.

With the detection methodology established and summarized in Figure 5, the parameters AT, RT and TR for the application of the alerting method must be defined. Also, the performance of the methodology with this set of parameters (and possible variations) must be assessed in terms of detection of previously known threatening gradients and impact on the availability of a supported GBAS facility. The results from this assessment will be presented and discussed in Section 6.

The proposed method involves a set of parameters that need to be assessed. For example, considering the Alert Threshold (AT) parameter, it is expected that lower thresholds will be more sensitive in detecting ionospheric irregularities. On the other hand, high sensitivity can generate frequent alerts that may be unnecessary, excluding satellites and significantly degrading GBAS availability. AT is considered the most critical parameter because it has a major impact on system performance. The Recovery Threshold (RT) and Time to Recover (TR) parameters of the alerting methodology will act together, directly impacting the time it takes for satellites to be readmitted to the GBAS solution. Higher values for RT are more permissive and allow for more prominent gradient variations. The TR parameter directly affects the availability of the satellites since it will determine the delay before possible satellite readmission. Thus, longer TRs will result in less availability in general.

For both datasets, combinations of these three parameters were tested using the values expressed in TABLE 2, which shows the values tested for each parameter in each column. Hence, this table should not be read row by row. Instead, all the combinations of values for AT (5), RT (2), and TR (3) parameters were tested, resulting in 30 different alert parameter combinations. The results of the alerting method were also analyzed considering the periods of time in which each satellite is under an "alert" condition, if any.

An example for a satellite arc in Sao Jose dos Campos cluster (SJ) is presented in Figure 6 with the alert periods separated in different colors to express if they were detected by the test statistic (pink) or the data gap (orange) criterion. For this performance evaluation, all periods identified by the method are counted, regardless of the criteria by which they were detected. Figure 6 includes all analyzed elements, including a validated gradient from the Brazilian threat model at the time it was detected.
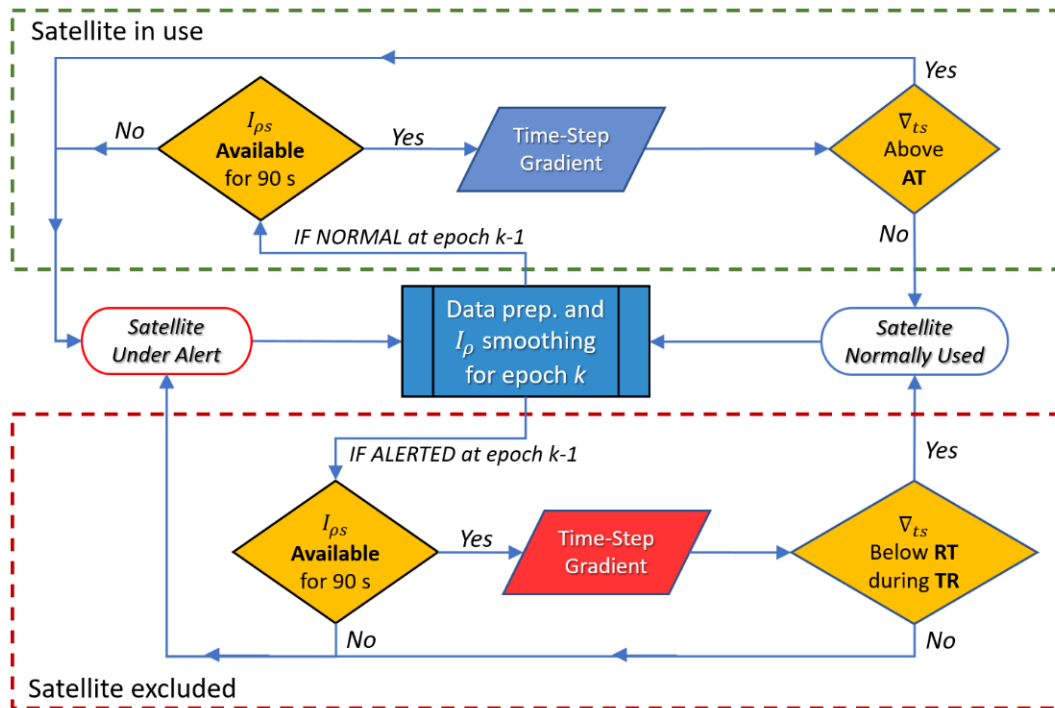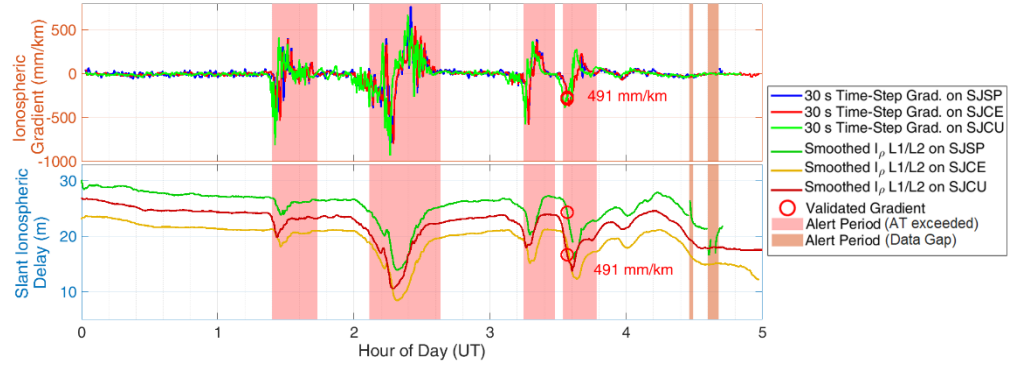

Figure 5
Processing flow chart with the verifications of the alerting system for one satellite at one monitoring station

Alert Thresh. **AT** (mm/km)	Recovery Thresh. **RT** (mm/km)	Time to Recover **TR** (min.)
200		
250	100	5
300		10
350	150	15
400		

Figure 6

Time-step gradients (upper panel) and respective slant ionospheric delays (lower panel) for PRN 01 on March 7, 2014, with the detection periods using parameters AT: 300 mm/km; RT: 100 mm/km; TR: 5 min. at the SJ cluster. Red circle indicates the occurrence time of a validated gradient, which in this case was detected by the alerting method.

The results were analyzed by checking if the method with the evaluated set of parameters could detect known station-pair gradients. In the example of Figure 6, a gradient of 491 mm/km validated as contributing to the Brazilian ionospheric threat model was declared as detected by the alerting parameters shown in the plot header since the periods where alerts are shown contain this gradient. Additionally, considering a GBAS facility sited at a reasonable distance from the alerting stations, loss of availability was assessed for each set of parameters. Assuming that the affected satellite is excluded when an alert is issued, loss of availability was considered as the exclusion of three or more simultaneous satellites. Hence, the next section will present all results expressed in terms of detection performance and availability loss.

## 6 RESULTS AND DISCUSSION

6.1 Performance Metric

In a first approach, performance evaluation was made considering rigorously the alert periods detected by the proposed method using data gaps and the test statistic with the combination of parameters described above. However, in some cases, the proposed method triggered alerts a few minutes after the time of the threat model gradient. Such behavior suggests the alerting method can detect gradients from this dataset, although a couple of minutes later (typically 5 or 10 minutes if not within the original alert period) when compared to the time of the threat model gradient observation. The results without such tolerance periods are presented in Subsection 6.2. Based on this observation, subsequent detection performance evaluation assumed periods of tolerance for the alerts. Tolerance periods represent allowed delays between the occurrence of a significant ionospheric event identified in the threat model dataset and an alert being issued regarding it. In operational terms, taking 5 or 10 minutes to detect and alert an aircraft about a threatening condition is probably unacceptable. However, actual response time is associated with the distance and distribution of the monitoring stations relative to the GBAS facility location. These aspects are not discussed in this paper because the available data is historical and collected at limited times within the 11-year solar cycle. Investigations about the distance and distribution of the monitoring stations would require a specific campaign during the solar maximum, which is not feasible with the available data. Additionally, the reference dataset has limitations in terms of data quality and completeness since only a single gradient is identified and validated during a longer ionospheric event. Considering variable tolerance times in the performance analysis (as a sensitivity parameter) is an option to mitigate such limitations.

Hence, the periods of tolerance considered are within the interval between 5 and 20 minutes in steps of 5 minutes. Then, each set of parameters is evaluated by a score varying from 0 (gradient not detected) to 100 based on the classification presented in TABLE 3. The assessment algorithm expands the beginning of the alert periods by the tolerance time specified in TABLE 3 and checks whether each threat model gradient lies within a particular detection zone. This is illustrated in Figure 7, where t_{as} is the time when the alert starts. As an example, if a given alert period starts 8 minutes after a known validated gradient from the dataset, then it lies within detection zone 2 (representing a tolerance period between 5 and 10 minutes). Hence its score is 50. In a different example, if a given alert period starts 2 or 3 minutes after the validated gradient, it is classified in detection zone 1 and it receives a score of 100.

TABLE 3
Score defined for each detection zone and range of tolerance times

Detection zone	Tolerance time (minutes)	Score
1	0 – 5	100
2	10	50
3	15	20
4	20	5
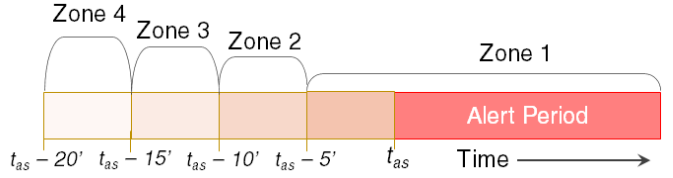
Figure 7
Detection zones based on tolerance times considered in alerting performance assessment

The same will happen if the alert period starts beforehand as long as the alert is maintained until the gradient occurs. In other words, the scores are attributed by determining if the gradient from the threat model database table is within the alerted periods, considering that they are expanded (only in advance) by each tolerance time.

An example to illustrate the tolerance time, which is an expansion of the alert periods for the purposes of analysis, is provided in Figure 8. This figure shows the test statistic for two stations in the upper panel, the validated gradient from the threat model, and the smoothed ionospheric delay in the lower panel. The red shaded area is the alert period determined by the test statistic using the parameters AT: 400 mm/km, RT: 100 mm/km and TR: 10 minutes. Three candidate tolerance times are represented by black dashed lines showing the time before the alert period starts.

First, the alert period is extended to start 5 minutes earlier, and it is determined whether or not this alert period contains the threat model gradient. If the gradient is not found, the alert period is extended to start 10 minutes earlier than the original period. If the gradient is not contained within this new period, then it is extended again in 5-minute steps until a maximum of 20 minutes.

For the specific case illustrated in Figure 8, the threat model gradient is not within the 5-minute tolerance, but within detection zone 2 according to Figure 7. Since the threat model gradient is within the 10-minute tolerance period, the score for the indicated set of parameters will be 50 for this gradient according to the scoring system in TABLE 3. Thus, the final score $\overline{Score_p}$ for each set p of parameters is the average of the scores of each gradient g from the dataset containing N_g threatening gradients:

$$\overline{Score_p} = \sum_{g=1}^{N_g} \frac{Score_g}{N_g} \tag{4}$$

This technique of computing scores was used to generate a single metric to evaluate the overall performance for each of the 30 combinations of the three parameters (AT, RT and TR). With the same set of parameters applied to all clusters in the entire dataset, 72 gradients from the threat model were evaluated by each combination, resulting in 30 different metrics to be compared.
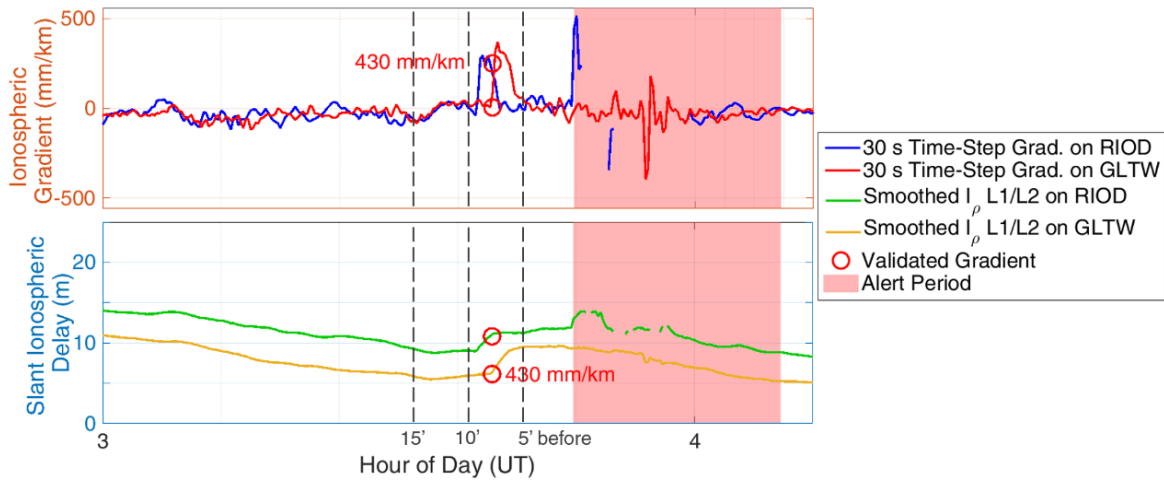
Figure 8
Example of tolerance times in detection analysis at the RJ cluster for GPS PRN 27 on Dec. 31, 2013, using the alerting parameter combination as AT: 400 mm/km, RT: 100 mm/km, and TR: 10 minutes

Note that the scores used to measure the performance of each parameter combination do not necessarily represent the percentage of gradients detected but instead provide a measure for the entire dataset that considers not only if the gradient was successfully detected but if it was detected within a given tolerance time. In other words, the scores also consider how late the alert was issued after a known threatening event occurred (if an alert was not issued before the event), attributing higher scores to shorter tolerance periods, since the sooner the threatening gradient is detected, the better is the performance in terms of protecting integrity. Importantly, tolerance times are only used to assess the methodology on this specific dataset – they are not part of the method itself.

6.2 Results

Station-pair and time-step gradient estimates have different characteristics. Also, the available dataset has limitations in terms of completeness of results and receiver robustness, such as using a single point in time to represent an ionospheric event. To mitigate such limitations, tolerance periods were considered with the scoring system presented in TABLE 3. However, before computing scores, the detection results were analyzed for each tolerance time to check their effect for each combination of parameters.

In Figure 9(a), performance is presented showing the percentage of detected gradients for each tolerance time. Bins of the same color represent the same parameter combination, as shown in the figure legend. As indicated in the top left corner of the plot (upper panel), each combination has five bins representing the five tolerance periods, which vary from 0 to 20 minutes at 5-minute steps.

The first aspect to note from Figure 9(a) is that all parameter combinations can achieve the same maximum percentage of detected gradients (97%) within a tolerance time varying from 5 to 20 minutes, increasing from the more sensitive sets to less sensitive parameter combinations (as explained in Subsection 6.1). The 3% of gradients not detected by any combination with any tolerance time correspond to two different events that will be discussed in Subsection 6.3.

The results from Figure 9(a) show that considering a tolerance time of at least 5 minutes encompasses more gradients, significantly improving the final performance. The clearest example of such behavior is seen in the last six groups of Figure 9(a) corresponding to the combinations with AT of 400 mm/km. Without allowing for tolerance time results in 76% of gradients detected. With a tolerance of 5 minutes for the same parameters, 89% of gradients are detected, corresponding to 9 more gradients detected. Increasing the tolerance time to 10 minutes, the detection of gradients grows to 94%, and it reaches 97% for a tolerance time of 20 minutes.

It is possible that an ionospheric event identified in the dataset may not be the same event that triggered the alerting method 10 or 20 minutes later. Nevertheless, notwithstanding the limitations of this dataset which were previously discussed, except for the two undetected gradients that will be further discussed in Subsection 6.3, in 100% of the cases in which the alerting method did not detect the threatening gradient in the resulting alert period, an alert was triggered within a maximum of 20 minutes, depending on the alerting parameters used.
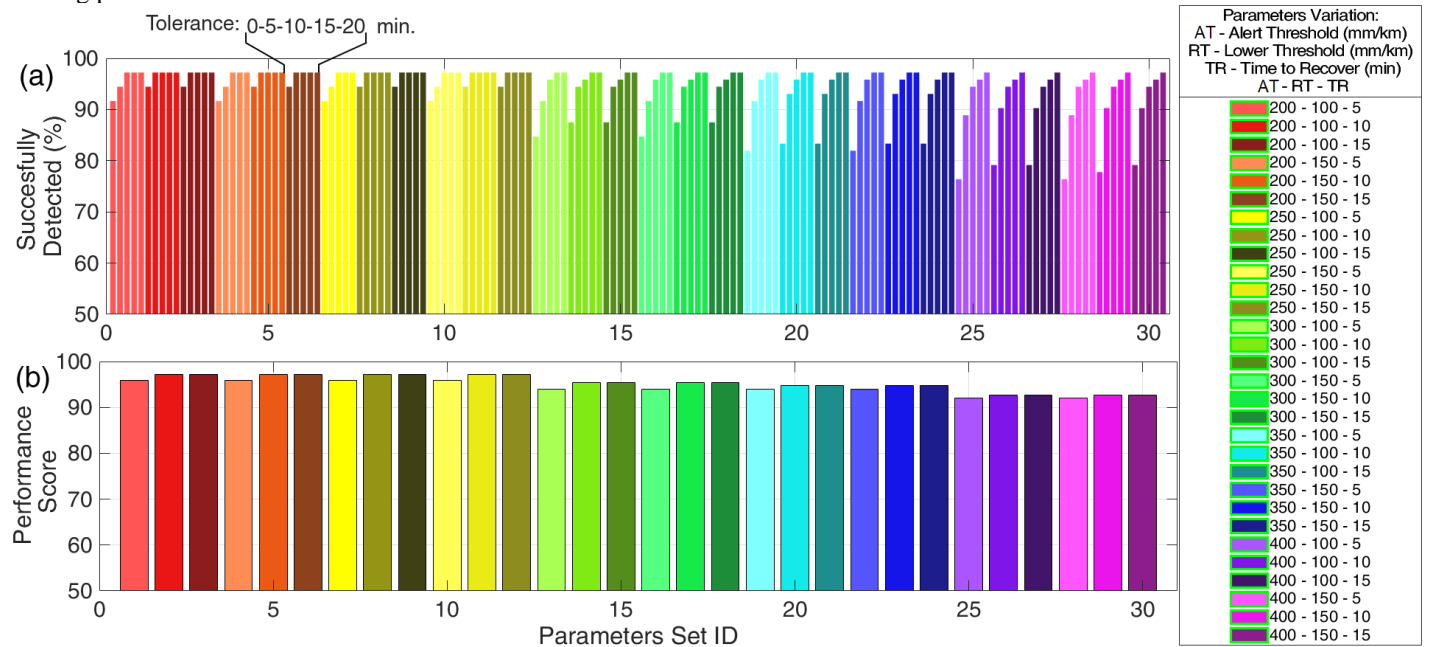

Figure 9

Performance results of the alerting methodology using all parameter combinations considering gradients detected by at least one monitoring station. (a) Percentage of detected gradients within tolerance times. (b) Performance score for each parameter combination

This behavior shows that the combination of data gaps and time-step gradients have sufficient sensitivity to detect threatening station-pair gradients, although with some delay. This delay, if considered significant, can be mitigated by distributing monitoring stations at longer distances from the GBAS facility and/or with a more favorable configuration. As previously stated, the distances and orientation of the monitoring stations relative to GBAS facilities could not be investigated in this paper and is left for future work.

The results using the scoring system based on the tolerance times from TABLE 3 are presented in Figure 9(b), showing the overall performance exceeding 90% for all parameter combinations. The performance of all parameter sets is quite similar, with a score of 97 for the best performance and the worst around 93. In both panels of Figure 9, it is noted that the RT parameter showed no difference when varied by itself (with the other two parameters kept the same).

Taking advantage of the results shown in Figure 9, an additional clarification of how applying the scoring system as a performance metric can be provided. The results from Figure 9(b) can also be obtained by averaging the data from Figure 9(a). In other words, each five bars of the same color in Figure 9(a) will become a single bar of the same color in Figure 9(b). The best detection results of 97 in the scoring system mean that the vast majority of gradients were detected within the alert period or with some delay.

Choosing the optimal set of parameters for detection is not straightforward since the loss of availability resulting from a specific combination of parameters must also be taken into account. The availability assessment will be discussed in Subsection 6.4. Additionally, the available dataset is noticeably heterogeneous, having monitoring stations in significantly different regions with distinct ionospheric characteristics. Considering only performance as a criterion, based on Figure 9(b), the set of parameters with the best performance for the dataset as a whole while being likely to result in higher availability (i.e., high AT and RT with short TR) is the combination 250-150-10 respectively for AT-RT-TR.

Due to the heterogeneity of the dataset, the two clusters with the largest number of gradients from the Brazilian Threat Model dataset were investigated. The Salvador cluster (SV) has 31 identified gradients distributed over 26 different days, and the Sao Jose dos Campos cluster (SJ) has 24 threat model gradients distributed over 10 days. The same scoring system was applied only to the events in each cluster. Thus, the performance for each cluster also took into account the tolerance times to classify the detections and compute the performance scores as proposed. In this evaluation, more than a third of the parameter sets achieved scores of 100, with the worst scores of 95 for the SV cluster. For this case, the least sensitive parameter set with the best performance results is the combination 350-150-10 respectively for AT-RT-TR. However, in the SJ cluster, no combination could achieve a score of 100, and the least sensitive combination with the best results is the set 250-150-10 for AT-RT-TR with a score of 96%, agreeing with the results for the entire dataset. The SJ cluster could not achieve a 100 score because one gradient was not detected by any set of parameters. This specific gradient will be briefly discussed in Subsection 6.3.

The different optimal thresholds obtained from the two presented clusters located far apart in regions with distinct ionospheric characteristics suggests the ideal set of parameters must be analyzed and adapted for each region. However, if the same values have to be used for different regions, a more conservative approach shall be adopted with the best overall integrity results, even if it is too sensitive (sacrificing availability) for some regions.

When analyzing the performance results in Figure 9, the best detection results are obtained for more sensitive parameter sets. In particular, the best detections result with the largest AT are achieved for the combination 250-150-15 respectively for AT-RT-TR with a final score around 97, and performance slowly degrades until the least-sensitive (higher AT) combination 400-150-5 is reached, with a final score around 93. However, this is not the final word. Choosing the best set of parameters should not only consider the performance results but also consider the loss of availability caused by each combination, which will tend to favor less-sensitive choices.

6.3 Undetected gradients

The best results shown in Figure 9 detected 70 out of 72 gradients from the selected ionospheric threat model gradients within a maximum tolerance time of 10 minutes, meaning that two gradients were not detected by the proposed method by any combination of parameters. One of the undetected gradients occurred due to a receiver fault not detected by the screening process. The fault occurred in the MC cluster when tracking GPS PRN 27 around 2 am (UTC) on February 11, 2014. . The second threat model gradient not detected by any combination of parameters and any tolerance time was measured by stations SJCU and SJCE for GPS PRN 03 on February 15, 2014. In this case, the detection analysis was performed using only these two stations that originally measured a gradient of 444 mm/km. It was observed that the ionospheric event not captured by the time-step method using a pair of stations from the cluster (SJCU and SJCE) was captured by a different pair of monitoring stations (with a third station introduced, SJSP) from the same cluster. This second undetected gradient analysis suggests that using only two monitoring stations around a GBAS facility is likely not sufficient to detect threatening gradients, requiring at least a third monitoring station. On the other hand, 70 out of 72 gradients from the adopted dataset were detected with a combination of parameters using only two stations in a cluster. The performance results from the dataset allow one to conclude that the time-step method used as a test statistic along with data gaps as criterion to detect threatening gradients performs satisfactorily in most cases.

6.4 Impact on availability

Excluding satellites from use by GBAS due to alerts causes loss of availability. It is expected that more sensitive parameters result in detection of more gradient events, whether threatening or not, which means they exclude satellites for longer periods and degrade availability. Hence, the choice of the optimal set of alerting parameters is a trade-off between detection performance and availability loss.

This availability assessment was conducted considering all stations that form each cluster depicted in Figure 4, following the single alert station rule. In other words, the alerts from all stations of each cluster were merged to generate the alert periods for each satellite. Assuming that these satellites are excluded from the broadcast GBAS correction messages during their alert periods, the availability analysis checked these for periods of simultaneous alerts for multiple satellites.

For this analysis, it was established that the exclusion of three or more satellites simultaneously results in the total outage of the system. Even though such an assumption might not match the results if an availability assessment were performed on an actual GBAS facility, this was the criteria applied in this work considering the available threat model data. Thus, to analyze the outages caused by each set of alerting parameters, a useful metric is obtained by summing the total time that three or more satellites were simultaneously excluded for each day in each cluster. Due to this metric's nature, this kind of analysis only makes sense if applied to each cluster individually. This is different from the detection performance evaluation reported previously, which used a single metric for the entire dataset.

Analyzing the outage time with the proposed metric is relatively straightforward when studying a single day. However, the ionospheric conditions along the days and clusters vary considerably. Hence, it is implausible that a single metric could adequately express the overall impact on availability. For this reason, outage analysis was performed for each day individually, regardless of how many ionospheric events were present in the day. Due to the large number of plots generated for this investigation, only the most relevant information is presented.

Figure 10 presents the days with the longest and shortest outage periods, respectively, in the dataset. In Figure 10 (a), the system is totally unavailable for approximately 5.5 hours in the worst case and approximately 3 hours in the best case. In Figure 10 (b), the outage periods vary across parameter sets from just over two hours to zero (meaning 100% availability according to the adopted metric).

These results are expected regarding the overall behavior of the outages with respect to the parameter combinations, as discussed in Section 5. Shorter periods of outages are obtained with higher values for AT. A few cases of more extended outages for higher AT, with RT and TR kept the same, occurred, but were due to specific conditions. TR is the parameter with the most consistent behavior among the combinations since it naturally extends the alert periods when higher values are employed.

Considering that Figure 10 shows the worst (longest outages) and best (shortest outages) cases among the validation dataset, all remaining resulted in outages with significant variability depending on day and location but were always between these two limits in terms of overall behavior.
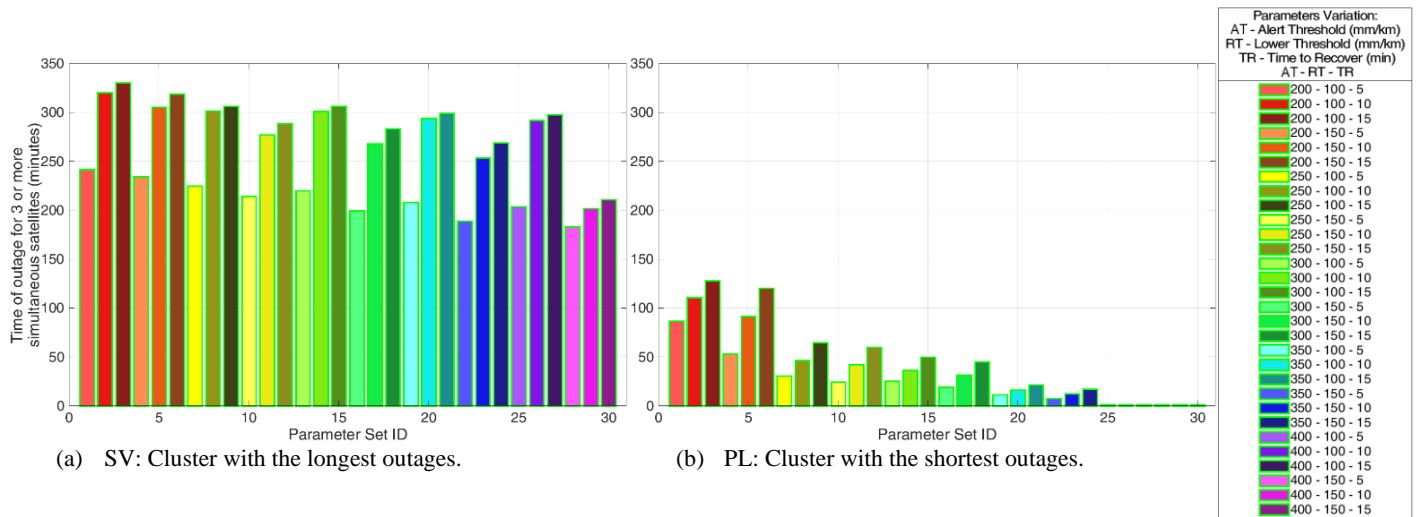

(a) SV: Cluster with the longest outages.
(b) PL: Cluster with the shortest outages.

Figure 10
Outages in SV (a) and PL(b) clusters on February 27 and 14, 2014, respectively from all sets of tested parameters

Because of the significant variability of outage times over the days and clusters of the dataset, the distribution of outages for each parameter combination was analyzed. The most noticeable conclusion from such an analysis is the large dispersion of outage durations. In general, the shortest outages are obtained from parameter sets with AT of 400 mm/km, reaching minimum outage durations of less than half an hour. The combinations with 200 mm/km AT yielded minimum outages at least twice this duration, but still with considerable variability depending on the day and location with respect to the geomagnetic latitude.

7 CONCLUSIONS

This paper develops a conceptual system along with a methodology to alert threatening ionospheric gradients in advance to support GBAS in low latitudes. The conclusion from the preceding analysis of the parameter combinations is that the proposed method effectively detects threatening gradients for a GBAS facility for many reasonable values of these parameters. Furthermore, even though the technique requires a non-obvious choice of parameters as thresholds and recovery triggers for the test statistic, the performance results proved that the vast majority of gradients were detected within a reasonable tolerance time.

Considering the adopted dataset, the best performance score was 97%, with the great majority of threatening gradients detected and alerted with a tolerance time of 5 minutes and all detected gradients detected with a maximum tolerance time of 10 minutes. Only two gradients from the dataset were not detected by the proposed technique. One of these is due to a receiver error not captured by the data screening process and the rules established to compute the test statistic. The other missed gradient was declared undetected when applying the criteria of the proposed method. However, it was detected by a neighbor station that was part of the same cluster using a more-sensitive combination of parameters.

The analysis of the two gradients that the proposed method failed to detect suggests three different actions to improve the alerting methodology. First, the data screening process could be reviewed and updated to make it more robust to the receiver errors apparent in these two datasets. Second, more robust monitor station receivers could be used that are less susceptible to faulty or inconsistent measurements, particularly during times of ionospheric disturbances. Third, three or more monitor stations should be used in each cluster, since two out of three stations were not able to detect a threatening gradient in the SJ cluster.

Regarding the loss of availability imposed by the alerting method, the results were significantly different for different clusters and days. Consequently, determining the optimal trade-off between detection performance and availability is not a straightforward task. For a safety-critical system like GBAS, the detection of threatening gradients must be the priority, even if this results in conservatively issuing more alerts than strictly necessary. Even though the worst outages exceeded 5 hours during nighttime, this loss of availability under threatening ionospheric conditions is far better than declaring the system totally unavailable every night. This improvement in low-latitude nighttime GBAS availability is a major contribution of this paper.

ACKNOWLEDGMENTS

REFERENCES

Affonso, B. J., Moraes, A., Sousasantos, J., Marini-Pereira, L., & Pullen, S. (2022). Strong ionospheric spatial gradient events induced by signal propagation paths aligned with equatorial plasma bubbles. *IEEE Transactions on Aerospace and Electronic Systems*, Early access, https://doi.org/10.1109/TAES.2022.3144622.

Caamano, M., Felux, M., Gerbeth, D., Juan, J. M., Gonzalez-Casado, G., & Sanz, J. (2019). Network-based ionospheric gradient monitoring to support GBAS. *Proc. of the 32nd International Technical Meeting of the Satellite Division of the Institute of Navigation, ION GNSS+ 2019*, *Miami, FL*, 2888–2902. https://doi.org/10.33012/2019.16926

Caamano, M., Juan, J. M., Felux, M., Gerbeth, D., González-Casado, G., & Sanz, J. (2021). Network-based ionospheric gradient monitoring to support GBAS. *NAVIGATION*, 8(1), 135–156. https://doi.org/10.1002/navi.411

Chang, H., Yoon, M., Lee, J., Pullen, S., & Marini-Pereira, L. (2019). Assessment of ionospheric spatial decorrelation for daytime operations of GBAS in the Brazilian region. *Proc of the 2019 International Technical Meeting of The Institute of Navigation, Reston, VA*, 618–631. https://doi.org/10.33012/2019.16673

Chang, H., Yoon, M., Pullen, S., Marini-Pereira, L., & Lee, J. (2021). Ionospheric spatial decorrelation assessment for GBAS daytime operations in Brazil. *NAVIGATION*, 68(2), 391–404. https://doi.org/10.1002/navi.418

Datta-Barua, S., Lee, J., Pullen, S., Luo, M., Ene, A., Qiu, D., Zhang, G., & Enge, P. (2010). Ionospheric threat parameterization for local area global-positioning- system-based aircraft landing systems. *Journal of Aircraft*, 47(4), 1141–1151. https://doi.org/10.2514/1.46719

Datta-Barua, S., Walter, T., Pullen, S., Luo, M., Blanch, J., & Enge, P. (2002). Using WAAS Ionospheric Data to Estimate LAAS Short Baseline Gradients. *Proc. of the 2002 National Technical Meeting of The Institute of Navigation, San Diego, CA,* 523–530.

Felux, M., Circiu, M.-S., Gerbeth, D., & Caamano, M. (2017). Future GBAS Processing - Do we need an ionosphere-free mode? *Proc. of the 2017 Intenational Symposium on GNSS (ISGNSS), Hongkong, China*, 11 –13.

Gerbeth, D., Circiu, M.-S., Caamano, M., & Felux, M. (2016). Nominal Performance of Future Dual Frequency Dual Constellation GBAS. *International Journal of Aerospace Engineering*, 2016, 1–20. https://doi.org/10.1155/2016/6835282

Jung, S., & Lee, J. (2012). Long-term ionospheric anomaly monitoring for ground-based augmentation systems. *Radio Science*, 47(4), 1–12. https://doi.org/10.1029/2012RS005016

Lee, J., Seo, J., Park, Y. S., Pullen, S., & Enge, P. (2011). Ionospheric threat mitigation by geometry screening in ground-based augmentation systems. *Journal of Aircraft*, 48(4), 1422–1433. https://doi.org/10.2514/1.C031309

Lee, J., Yoon, M., Pullen, S., Gillespie, J., Mathur, N., Cole, R., De Souza, J. R., Doherty, P., & Pradipta, R. (2015). w. *Proc.of the 28th International Technical Meeting of the Satellite Division of The Institute of Navigation (ION GNSS+ 2015), Tampa, FL*, 1500–1506.

Marini-Pereira, L., Pullen, S., Moraes, A. de O., & Sousassantos, J. (2021). GBAS operation in low latitudes - PART 1: Challenges, Mitigations, and Future Prospects. *Journal of Airspace Technology and Management*, 13(e4621), 1–24. https://doi.org/10.1590/jatm.v13.1236

Mirus. (2015). *Effects of Low Latitude Ionospheric Activity on Global Navigation Satellite Systems (GNSS)*. Final Report submitted to SDTP and USTDA, Wirtz, VA. Available at: https://www.icao.int/SAM/Documents/2016-PBNGNSS/Low%20Latitude%20Threat%20Model-Final-Jan15.pdf. Accessed on: 30 May 2021.

Pullen, S., Luo, M., Walter, T., & Enge, P. (2010). Using SBAS to enhance GBAS user availability: Results and Extensions to enhance air traffic management. *ENRI International Workshop on ATM/CNS (EIWAC), Tokyo, Japan*.

Salles, L. A., Vani, B. C., Moraes, A., Costa, E., & de Paula, E. R. (2021). Investigating Ionospheric Scintillation Effects on Multifrequency GPS Signals. *Surveys in Geophysics*, 42(4), 999–1025. https://doi.org/10.1007/s10712-021-09643-7

Sousasantos, J., Marini-Pereira, L., Moraes, A. de O., & Pullen, S. (2021). Ground-based augmentation system operation in low latitudes - Part 2: Space weather, ionospheric behavior and challenges. *Journal of Aerospace Technology and Management*, 13(e4821). https://doi.org/10.1590/jatm.v13.1237

Subirana, J., Zornoza, J., & Hernández-Pajares, M. (2013). *GNSS Data Processing, Vol. I: fundamentals and   algorithms.* Noordwijk: European Space Agency (ESA).

Yoon, M., Kim, D., & Lee, J. (2017b). Validation of Ionospheric Spatial Decorrelation Observed During Equatorial Plasma Bubble Events. *IEEE Transactions on Geoscience and Remote Sensing*, 55(1), 261–271. https://doi.org/10.1109/TGRS.2016.2604861

Yoon, M., Kim, D., & Lee, J. (2020). Extreme ionospheric spatial decorrelation observed during the March 1, 2014, equatorial plasma bubble event. *GPS Solutions*, 24(2), 1–11. https://doi.org/10.1007/s10291-020-0960-x

Yoon, M., Kim, D., Lee, J., & Pullen, S. (2015). Multi-dimensional verification methodology of ionospheric gradient observation during plasma bubble events in the Brazilian region. *Proc. of the Institute of Navigation Pacific Positioning, Navigation and Timing Meeting (Pacific PNT), Honolulu, HI*, 748–762.

Yoon, M., Kim, D., Lee, J., Rungraengwajiake, S., & Pullen, S. (2016). Assessment of equatorial plasma bubble impacts on ground-based augmentation systems in the Brazilian Region. *Proc. of the 2016 International Technical Meeting of The Institute of Navigation*, 368–379. https://doi.org/10.33012/2016.13423

Yoon, M., Kim, D., Pullen, S., & Lee, J. (2019). Assessment and mitigation of equatorial plasma bubble impacts on category I GBAS operations in the Brazilian region. *NAVIGATION*, 66(3), 643–659. https://doi.org/10.1002/navi.328

Yoon, M., Lee, J., Pullen, S., Gillespie, J., Mathur, N., Cole, R., de Souza, J. R., Doherty, P., & Pradipta, R. (2017a). Equatorial Plasma Bubble Threat Parameterization to Support GBAS Operations in the Brazilian Region. *NAVIGATION*, 64(3), 309–321. https://doi.org/10.1002/navi.203